Numerical SPH analysis of debris flow run-out and related river damming scenarios for a local case study in SW China

Anika Braun[a], Sabatino Cuomo[b, *], Stefano Petrosino[b], Xueliang Wang[a], Luqing Zhang[a]

a: Institute of Geology and Geophysics, Chinese Academy of Sciences, No. 19 Beitucheng Western Road, 100029 Beijing, China, AB: anika.braun@rwth-aachen.de (corresponding author), XW: wangxueliang@mail.ggcas.ac.cn, LZ: zhangluqing@mail.iggcas.ac.cn

b: Department of Civil Engineering, University of Salerno, Via Giovanni Paolo II 132, 84084 Fisciano, Italy, SC: scuomo@unisa.it, SP: petrosino.stefano@gmail.com

*: corresponding author

Keywords

Landslide dam, numerical modeling, forward-analysis, Smoothed Particle Hydrodynamics

Abstract

A smoothed particle hydrodynamics (SPH) numerical modeling method implemented for the forward simulation of propagation and deposition of flow-type landslides was combined with different empirical geomorphological index approaches for the assessment of the formation of landslide dams and their possible evolution for a local case study in southwestern China. The SPH model was calibrated with a previously occurred landslide that formed a stable dam impounding the main river, and it enabled the simulation of final landslide volumes, and the spatial distribution of the resulting landslide deposits. At four different sites on the endangered slope landslides of three different volumes were simulated, respectively. All landslides deposited in the main river, bearing the potential for either stable impoundment of the river and up-stream flooding scenarios, or sudden breach of incompletely formed or unstable landslide dams and possible outburst floods downstream. With the empirical indices none of the cases could be identified as stable formed landslide dam when considering thresholds reported in the literature, showing up the limitations of these indices for particular case studies of small or intermediate landslide volumes and the necessity to adapt thresholds accordingly for particular regions or sites. Using the occurred benchmark landslide as a reference, two cases could be identified where a complete blockage occurs that is more stable than the reference case. The other cases where a complete blockage was simulated can be considered as potential dam-breach scenarios.

Abbreviations

BI	Blockage Index
DBI	Dimensionless Blockage Index
DEM	Digital elevation model
DTM	Digital terrain model
IR	Relief Index
MOI	Morphological Obstruction Index
HDSI	Hydrodynamic Dam Stability Index
SPH	Smoothed Particle Hydrodynamics

1. Introduction

Landslides of the flow type, which are defined as flows or flow slides of various soil materials, such as debris, sand, silt, or clay, at different water saturation and plasticity levels (**Hungr et al. 2014)**, are particularly dangerous, as they can reach high velocities and long run-out distances, leaving the exposed individuals with little time to react. Moreover, landslides of the flow type are among those with a high potential for the formation of landslide dams (**Costa and Schuster 1988**). A landslide dam is defined as the partial or complete blocking of a river channel, leading to the impoundment of water (**Ermini and Casagli 2003**). Different hazard scenarios can arise from such a situation, ranging from short-term impoundment of water to large scaled flooding upstream or downstream outburst flood waves in case of spontaneous dam breach. In all these scenarios the most vulnerable areas are affected: the valley floors, being the base for inhabitation and lifelines in mountainous areas. The severity of such a hazard scenario depends largely on the degree of river blockage and the longevity of the impoundment, while these factors are controlled by characteristics of the landslide dam, such as height and volume, the landslide velocity, the characteristics of the dammed valley, such as its width, and characteristics of the impounded river, expressed e.g. through the catchment area, stream power, and river bed inclination (**Costa and Schuster 1988; Ermini and Casagli 2003; Tacconi Stefanelli et al. 2016**). Particularly in narrow valleys with steep slopes, already small landslide volumes can form dams and cause hazardous situations (**Costa and Schuster 1988**).

Due to the size of the areas that can be affected in up- or downstream flooding situations, it is difficult to account for this type of hazard in regional planning by avoidance strategies. However, it can be useful to study local cases with a high potential for the occurrence of dam forming landslides, e.g. by means of run-out modeling, for targeting slope stabilization and mitigation measures.

The existing literature addressing the hazard imposed by landslide dams in local case studies focuses mainly on longevity and breaching scenarios of a dam once it is formed (**Tacconi Stefanelli et al. 2015; Fan et al. 2017; Okeke and Wang 2016**). However, local case studies investigating whether a landslide has the potential to form a dam and block a river are scarce. For this purpose two steps would be necessary, firstly to perform landslide susceptibility analysis including the landslide propagation, run-out, and deposition, and secondly to discriminate whether the resulting landslide deposit can form a dam.

For the first step, methods for assessing landslide run-out (**Corominas et al. 2014**) can basically be grouped into empirical methods, where empirical relationships between landslide run-out and geometrical or morphological characteristics are established, and rational methods, which are based on mathematical models. In the context of landslide dams, **Fan et al. (2014)** have implemented an empirical method for landslide run-out estimation based on geomorphological characteristics for the prediction of coseismic landslide dam formation on a regional scale. While empirical methods of run-out modeling work well on a regional scale using large datasets for the model calibration, rational methods work well on a local scale. For landslides of the flow type, methods based on continuum mechanics, allowing for the coupling of mechanical and hydraulic behavior, discretized with the Lagrangian meshless smoothed particle hydrodynamics (SPH) approach (**Gingold and Monaghan 1977; Lucy et al. 1977**), have proven to be particularly useful (**Pastor et al. 2014**). Such an approach has been developed by **Pastor et al. (2009)**, and successfully implemented to case studies of landslides of the flow type for instance by **Cascini et al. (2014), Cuomo et al. (2014)** or **Pastor et al. (2014)**, and for the modeling of coseismic landslides forming landslide dams by **Huang et al. (2012)**.

With regard to the second step, the discrimination of river blocking and non-blocking landslides, previous studies focus mainly on empirical relationships among geomorphological and hydrological properties of the landslide, the affected valley, the riverbed and the river catchment that are characterized by geomorphological indexes. These studies are based on large inventories of landslide dams covering different evolution scenarios of the impoundment, for instance for New Zealand (**Korup 2004**), Italy (**Ermini and Casagli 2003; Tacconi Stefanelli et al. 2015**), China (**Fan et al. 2012; Peng and Zhang 2012**), or worldwide (**Costa and Schuster 1988**).

In this study we aim to implement a methodology for the assessment of landslide dam evolution scenarios for local cases of flow type landslides in a mountainous area in southwestern China. In a first step we employ a continuum mechanics based SPH code for the simulation of propagation and deposition of potential landslides on a highly susceptible slope. Here we employ a numerical model that was parameterized in a previous study through back-analysis of a benchmark landslide case at the same site (**Braun et al. 2017**). Then we use suitable geomorphological indexes for the evaluation of the simulated deposits regarding possible landslide dam formation and evolution scenarios.

2. Materials and methods

2.1. Landslide propagation and deposition analysis with the "GeoFlow_SPH" model

The analysis of landslide propagation in susceptible areas was performed through the numerical analysis of debris flow propagation and deposition, also including the potential landslide dam formation into the river. The "GeoFlow_SPH" model was used, which is a depth-integrated hydro-mechanically coupled model proposed by **Pastor et al. (2009)**, based on the fundamental contributions of **Hutchinson (1986)** and **Pastor et al. (2002)**. The propagating mass is considered as a mixture of soil, whose voids are completely filled by water. The velocity of the soil skeleton (v) and the basal pore water pressure (p^b_w) are the unknowns of the model. Both variables are defined as the sum of two components related to: i) propagation, and ii) consolidation along the normal direction to the ground surface.

The governing equations are extensively discussed by **Pastor et al. (2009)**, being those herein listed: i) balance of mass of the mixture – propagating along the slope and increasing due to bed entrainment – combined to the balance of linear momentum of pore water, ii) the balance of linear momentum of the mixture, iii) a kinematic relation between the deformation-rate tensor and velocity field, iv) rheological equation relating the soil-stress tensor to the deformation-rate tensor. Further details are also provided by **Pastor et al. (2014)**, **Cascini et al. (2014)**, and **Cuomo et al. (2014)**.

Appropriate simulation of pore water pressures is fundamental issue as they change in time and space, and still pose challenging tasks as far as landslide initiation, transformation from slide to flow, landslide propagation, and deposition **(Cuomo 2014)**. In the model here used, the vertical distribution of pore water pressure is approximated using a quarter cosinus shape function, with a zero value at the surface and zero gradient at the basal surface (**Pastor et al. 2009**), and the basal pore water pressure (p^b_w) is regulated by Eq. 1, where c_v is the consolidation coefficient:

$$\frac{dp_w^b}{dt} = \frac{\pi^2}{4h^2} c_v p_w^b \quad (1)$$

As for the rheological model, in the case of a pure frictional mass, the basal tangential stress is given by Eq. 2:

$$\tau_b = -\left((1-n)(\rho_s - \rho_w) g \cdot h \cdot \tan\phi_b - p_w^b\right) \cdot \mathrm{sgn}\left(\bar{v}\right) \quad (2)$$

where τ_b is the basal shear stress, n is the soil porosity, ρ_s is the solid grain density, ρ_w is the water density, g is the gravity acceleration, h is the mobilized soil depth, ϕ_b is the basal friction angle, p_w^b is the basal pore water pressure, sgn is the sign function and $\bar{v}$ is the depth-averaged flow velocity. The initial pore water pressure is taken into account through the relative height of the water, h_w^{rel}, which is the ratio of the height of the water table to the soil thickness, and the relative pressure of the water p_w^{rel}, that is to say the ratio of pore-water pressure to liquefaction pressure. Estimates of both parameters can be obtained from the analysis of the triggering stage or back-analysis of propagation of past landslides (**Cuomo et al. 2014**).

Bed entrainment is also considered in the model, i.e. increase of landslide volume due to the inclusion of soil, debris and trees uprooted from the ground surface during the flow propagation. Bed entrainment has been formerly documented as an important process either for debris flows (**Cascini et al. 2014**) or debris avalanches (**Cuomo et al. 2014**). Because of bed entrainment, the elevation of ground surface (z) diminishes, and its time derivative can be computed based on different so-called "erosion" models, providing empirical or physically based equations for the entrainment rate (e_r). **Pirulli and Pastor (2012)** and **Cascini et al. (2014)** provide comprehensive reviews of the entrainment models available in the literature. Here, the formulation proposed by **Blanc (2008)** and **Blanc et al. (2011)** is used:

$$\frac{\partial z}{\partial t} = -e_r = -h \cdot v \cdot K \cdot (\tan\theta)^{2.5} \quad (3)$$

where v is the flow velocity, h the propagation height, θ is the slope angle, K is an empirical parameter to be calibrated, and the exponent equal to 2.5 is purely empirical and results from the analysis of experimental data (**Blanc, 2008**).

The equations are reduced from 3D to a quasi-3D formulation through a depth integration approximation, which is suitable for flow-like landslides because of a low ratio of the soil thickness to the landslide length. This quasi-3D depth-integrated model is both accurate (**Cascini et al. 2014; 2016**; **Cuomo et al. 2014; 2016**) and less time-consuming than a fully 3D model.

The SPH method is used to discretize the propagating mass into a set of moving "particles". It allows using a set of ordinary differential equations, while the information such as the unknowns and their derivatives are linked to the particles. The accuracy of the numerical solution and the level of approximation for engineering purposes depend on how the nodes are spaced and on the detail of the digital terrain model (DTM), as shown by **Pastor and Crosta (2012)** and **Cuomo et al. (2013)**.

The "GeoFlow_SPH" model was recently used for the back-analysis of the propagation and bifurcation of the above mentioned Tsing Shan debris flow, which occurred in 2000 in Hong Kong (**Pastor et al. 2014**), and for simulating the interplay of rheology and entrainment during the inception of debris avalanches (**Cuomo et al. 2014**). Similarly as in both these papers, the frictional rheology is here used because it is a reasonable and effective schematization for mixtures of coarse-grained soils saturated with water. Compared to other models from the literature (e.g. **McDougall and Hungr 2004**), the GeoFlow_SPH model has the principal merit to explicitly introduce the hydro-mechanical coupling between the solid skeleton and interstitial (pore water) pressure, the latter one being variable within space and time.

2.2. Landslide dam evaluation with geomorphological indices

The potential of landslides to form dams and their longevity are mostly analyzed through geomorphological indices, usually expressed as logarithms of the ratio between a characteristic describing the landslide dam and a characteristic describing the erosive power of the river. The characteristics of extensive databases containing different landslide dam evolution scenarios are plotted on bi-logarithmic plots to graphically identify domains of landslide dam formation and non-formation, usually around a domain of uncertain discrimination, and derive thresholds of the indices for the respective domains.

The "Blockage Index" (BI) proposed by **Swanson et al. (1986)** is defined as the ratio between the volume of the landslide dam V_d (m^3) and the catchment area A_b (km^2) above the point of blockage:

$$BI = \log\left(V_d/A_b\right) \quad (4)$$

While **Ermini and Casagli (2003)** suggested BI = 3.0 as lower threshold for the formation of a dam and BI = 5.0 as lower threshold for the formation of a stable dam based on a worldwide dataset, **Tacconi Stefanelli et al. (2016)** proposed BI = 3.0 as lower threshold for dam formation and BI = 5.68 lower threshold for the formation of a stable dam, based on a database for Italy.

A "Dimensionless Blockage Index" (DBI) was suggested by **Ermini and Csasgli (2003)**, who also introduced the height of the landslide dam H_d (m) as follows:

$$DBI = log\left(\frac{A_b \cdot H_d}{V_d}\right) \quad (5)$$

They propose DBI = 2.75 is indicated as the lower boundary of the stability domain and DBI = 3.08 as the lower boundary of the instability domain based on the worldwide dataset **(Ermini and Casagli 2003)**, while **Tacconi Stefanelli et al. (2016)** propose DBI = 2.43 as the lower boundary of the stability domain and DBI = 3.98 as the lower boundary of the instability domain.

A new system of indices was developed by **Tacconi Stefanelli et al. (2016)**, who proposed a "Morphological Obstruction Index" (MOI) to discriminate whether a landslide can basically form a dam that blocks the river or not in a first step, and the "Hydromorphological Dam Stability Index" (HDSI) to characterize the long-term stability of the dam in a second step. The MOI and HDSI indexes are defined as:

$$MOI = log(V_l/W_v) \quad (6)$$

$$HDSI = log\left(\frac{V_l}{A_b \cdot S}\right) \quad (7)$$

where the total volume of the landslide is V_l (m^3), as descriptor of the landslide characteristics and the width of the valley is W_v (m), as descriptor of the river characteristics; the local longitudinal slope of the channel bed S (m/m) is introduced to account together with the catchment area A_b for the erosive force of the river, i.e. the stream power.

Based on their database for Italy **Tacconi Stefanelli et al. (2016)** showed that the new indices enable a more clear discrimination of the different domains that the BI or DBI according to the procedure sketched in Fig. 1. They propose for the MOI a lower boundary of MOI = 3.00 for the formation of a dam with an uncertain evolution and MOI = 4.60 as lower boundary for the certain formation of a dam. Once a dam is formed (MOI > 4.60), the HDSI can be used to assess its longevity, and **Tacconi Stefanelli et al. (2016)** propose HDSI = 5.74 as the lower boundary for the formation of a stable dam with an uncertain evolution and HDSI = 7.44 as the lower boundary for the formation of a stable dam.

Figure 1.

3. The case study

3.1. Geological setting

The study area is located in Ningnan, a county in the south of Sichuan province in southwestern China (Fig. 2). Ningnan lies within an almost N-S trending mountain chain at the south-western boundary of the Sichuan Basin and the south-eastern margin of the Tibetan Plateau reaching peaks of up to 4790 m. Climatically the region is characterized as warm temperate with dry winters, a mean annual precipitation of 1025 mm, and a rainy season between June and September where usually more than 70% of the annual rainfall occurs.

Geologically this region is characterized by the complicated tectonic transformations it underwent. While being located at a continental margin from Paleozoic to Mesozoic times with the deposition of continental flood basalts in Permian and marine clastic-carbonate sequences from Silurian to Triassic, it transformed into a collisional orogeny during late Triassic and Cenozoic times, and terrestrial fluvial and lacustrine red bed facies were deposited (**Deng et al. 2014**). In Ningnan these sedimentation milieus led to the deposition of limestone, dolomite, mudstone, sandstone, and interbedded formations of these lithologies from Sinian throughout the Cambrian, Ordovician, Silurian, and Devonian times, and from Permian to Jurassic times (Fig. 3). Basalts, which crop out in the north and the east of the study area, were deposited during Permian. Local Quaternary deposits consist of loose sediments. The elevation in Ningnan county ranges between 600 m and 4,000 m, with steep slopes of over 60°.

Due to the rough terrain and the climatic conditions favoring strong rock weathering, especially of the young sedimentary rocks, and saturation of slopes during the rainy season, high seismicity due to the ongoing orogenesis, and interactions of human activities with the fragile slopes, the region is highly prone to landslides.

Figure 2.

3.2. Baishuihe landslide

The benchmark case for this numerical modeling study, Baishuihe landslide, is located in the north of Ningnan county, at 27.296283 N and 102.566979 E. Baishuihe is a complex landslide that started with several slumps within sandstone/mudstone interlayers above a dolomite layer (Fig. 3), both layers dipping in slope direction, that transformed into a debris flow. According to local villagers the slumps started developing in 2006, while the first main debris flow event happened in June 2012 after heavy rainfall, interrupting the main road along the valley. Then, in August 2012, another debris flow occurred after high cumulative rainfall, blocking the road again and damming the river, which resulted in a 4 m water level rise upstream, two fatalities, three persons missing, and damage to 38 houses. In the following years, intermittent small and medium scaled events were reported, with two larger ones in September 2015 and May 2016 after heavy rainfall. An engineering control structure has been put into place in the meantime, channelizing the debris to the left and the right in order to prevent the formation of major road blockings and river dams.

Baishuihe landslide consists of three major zones, a main deformation and source zone, a propagation zone, and a deposition zone (Fig. 4a). Being located at an elevation between 1615 m and 2100 m above sea-level, the main deformation zone stretches for about 400 m in N-S direction and 250-300 m in E-W direction, with a main scarp at the front and several other major cracks, shear- and tensile-failures with different degrees of deformation in the area above. The thickness of the deformation zone was estimated to be between 15.0 m and 26.7 m, with a mean thickness of 18 m and a volume of 1,700,00 m^3, while the volume of the main failure was estimated to be about 540,000 m^3. The propagation zone stretches between an elevation of 1,150 m and 1,820 m, covering an area of about 140 × 1070 m, with an average thickness of 4 m and a volume of approximately 600,000 m^3. Finally, the deposition zone consists of a T-shaped debris accumulation fan, stretching over a length of 300 m in sliding direction and about 580 m along the river valley, with an average thickness of 10 m, and an approximated volume of 870,000 m^3. Although the volume of the landslide is small, due to the narrow shape of the valley with steep slopes on both sides with slope angles between 30° and 50°, it was however able to dam the relatively shallow river, with an estimated depth of 3 m to 4 m, during the rainy season. Moreover, field evidence of run-up on the opposite slope indicates that the run-out of the landslide was limited by the valley shape (**Braun et al. 2017**). According to the classification of **Costa and Schuster (1988)** the dam formed by Baishuihe landslide can be characterized as Type III dam, where the dam fills the valley from side to side and the material also travels up- and downstream, which is typical for flows and avalanches. The formed, stable dam impounded the main river, leading to a rise of the river level of 4 m. However, since the dam was eventually removed by the local authorities a few days later, the long-term stability of the Baishuihe landslide dam is unknown.

The sliding material is according to field observations and laboratory analyses mainly composed of rocks and debris from the Ordovician interlayered sandstone/mudstone strata, containing 55% to 70% gravel (2 cm to 8 cm), 15% stones (20 cm to 30 cm), sandy soil, and occasional boulders with a size of up to 3 m (Fig. 4b-c). Fragments of material from the dolomite strata that forms the propagation zone indicate the occurrence of bed entrainment during the sliding process. The shear zone is composed of 55% clayey soil breccia, which consists of well-sorted particles between 2 mm and 5 mm, 20-25% clay, and 20-25% silt and sand.

Figure 3

4. Input data and analyses performed

4.1. Parameterization of the landslide propagation model

In a previous study a back-analysis has been carried out in order to estimate the mechanical behaviour (rheology) of Baishuihe landslide using the "GeoFlow_SPH" code (**Braun et al. 2017**). For this analysis the area indicated as "source 1" in Fig. 3 was assumed as landslide triggering area, varying the height of the triggering mass within the values recorded in the field, and thus considering different initial volumes. Moreover, the ratio of water table height to soil thickness h_w^{rel}, the ratio of pore water pressure to liquefaction pressure p_w^{rel}, the consolidation factor c_v, and the empirical factor for bed entrainment K were varied in different runs of the simulation. The field observations of the landslide geometry as given in 3.2, particularly of the width, height, and volume of the resulting deposit, were used for the rheological parameters optimization. Purposely, a newly defined multi-criteria procedure described above was used, based on the best-fitting of all the relevant geometrical features of landslide propagation. Input parameters and simulation results of the optimized model are listed in Table 1. The results of the back-analysis elucidated some interesting finings about the landslide mechanisms as well. In contrast to the initial idea that the landslide was triggered at full saturation of the soil in the source area, the model showed that it was actually initiated before full saturation of soil thickness was achieved at a relative height of water table to soil thickness of 0.5. Complete liquefaction of soil at the source area was also excluded, as the best-fitting run was for a pore water pressure to liquefaction pressure ratio of 0.6 and by implying a factor for bed entrainment of 0.006 the model showed that bed entrainment is a key factor, which is also evidenced by findings in the field where fragments of the dolomite layer constituting the propagation zone were found within the deposited material. Moreover, a triggering height of 15 m resulted in an initial volume of approximately 550,000 m^3, which is in accordance with the 540,000 m^3 estimated based on field observations, while the final volume of 912,255 m^3, the deposition width of 615 m, and a mean deposition height of 11 m are also in satisfying agreement with the field observations.

Table 1

4.2. Forward analysis of landslide propagation

On a stretch of roughly 3 km along the main valley south of Baishuihe landslide similar conditions are present: a very steep slope, the geological contact between the highly weathered sandstone/mudstone interlayers above the dolomite formation at an elevation of 1800 m to 1900 m dipping in slope direction. The occurrence of future collapses and the subsequent initiation of debris flow slides on the highly susceptible slope has to be considered a likely scenario. In order to assess the potential of the formation of landslide dams in case of a future landslide through forward simulation, simple geological and geomorphological landslide susceptibility analyses were performed through expert-judgment procedures, classifiable as "basic" methods according to **Fell et al. (2008)**. Thus, four potential triggering areas were individuated at the same elevation as the benchmark case landslide along the geological contact, assuming a similar shape and area in order to simulate a similar volume. Those landslide triggering susceptible areas were assumed as source zones for a forward analysis with the "GeoFlow_SPH" code, employing the previously back-analyzed landslide parameters (Figs. 4-5). As input for the back-analysis as well as the forward simulations a digital terrain model (DTM) with a horizontal resolution of 5 m was interpolated from 20 m contour lines. The simulation outputs are consequently also in a 5 m resolution.

Figure 4

Figure 5.

4.3. Landslide dam analysis

In order to discriminate between potential landslide dam formation and evolution scenarios for the simulated landslides we computed the above introduced indices for all simulated scenarios as well as for the benchmark Baishuihe landslide as a reference for a formed and stable river blockage with an uncertain evolution. As inputs the characteristics concerning the landslide itself, thus, the final landslide volume V_l, the volume of the landslide dam V_d, and the height of the landslide dam H_d were derived from the simulation results, using the median dam height defined as the value separating the higher half of the landslide dam height cells from the lower half as the input for the DBI. Regarding the river characteristics, the valley width W_v was derived from the DTM and the river channel width W_R was measured in Google Earth for each point of blockage (Fig. 6), whereas the valley/river cross section with the peak of the simulated dam height was considered as point of blockage, respectively. The catchment area A_b and the local longitudinal slope of the channel basin S were derived from a digital elevation model (DEM) in a geographic information system (GIS). For this purpose a DEM with a horizontal resolution of 30 m was obtained from the Japanese Aerospace Exploration Agency (JAXA) Advanced Land Observation Satellite (ALOS) Mission (**JAXA 2016**) covering the entire catchment area draining into the considered points of blockage (Fig. 2). Voids in the elevation data were filled with data from the National Aeronautics and Space Administration (NASA) Shuttle Radar Topographic Mission (SRTM), also with a 30 m horizontal resolution (**USGS 2015**). In ArcGIS the void-less DEM was first transferred into a depression-less DEM by filling all sinks and then a raster of accumulated flow was derived in terms of number of cells that drain into each cell of the raster. The flow accumulation was assessed for each point of blockage and multiplied by the cell size (30×30 m^2) to obtain the area draining into the considered points of blockage. The same elevation data was used to assess the local longitudinal slope of the channel bed, up to 1 km upstream for each point of blockage.

Figure 6.

5. Results and Discussion

5.1. Simulation results

The simulated triggering heights h_{trig}, initial landslide volumes V_i, final landslide volumes V_f, landslide dam volumes V_d, and landslide dam heights H_d are given in Table 2 and Table 3 for the benchmark case Baishuihe landslide and the twelve different cases for the four assumed source zones. The resulting soil heights of the landslide deposits are shown in Fig. 7 and Fig. 8 in spatial context. As expected, the initial landslide volumes increase with increasing triggering height, so at a triggering height of 10 m the initial landslide volume is between 361,000 m^3 and 365,500 m^3, at a triggering height of 15 m it is between 541,500 m^3 and 550,125 m^3, and at a triggering height of 20 m between 722,000 m^3 and 731,000 m^3. The final landslide volumes increase with increasing run-out distance, and while at sources No. 2 and 3 the final volume is around 1.5 times the initial volume, it is around the 2.25 fold of the initial volume at source No. 4 and the 3.35 to 4.21 fold at source No. 5.

While for sources No. 2 and 3 the entire final volume of the landslide was deposited in the river channel in all scenarios, for source No. 4 part of the final volume ran up the opposite slope and for source No. 5 part of the landslide material already deposited on the propagation path within a tributary gully (Fig. 7 and Fig. 8). Thus, for sources No. 2 and 3 the final landslide volume was also assumed as landslide dam volume, while for sources No. 4 and 5 only the volume of the material deposited within the river channel bed was considered as dam volume (Table 2).

It is interesting to compare the resulting landslide deposits for source No. 2 and No. 3 (Fig. 7). In both scenarios the landslide enters the river channel through the same gully, but while for source No. 2 the landslide spreads over a long distance of the river channel and forms a wide and shallow landslide dam, the width increasing with increasing volume, for source No. 3 the deposited material forms a very condensed, steep and high landslide dam where the maximum height is increasing with increasing volume (Tab. 2, Fig. 7). It is generally expected for the landslide dam height to increase with increasing landslide volume. However, as the aforementioned example shows, flow-like landslides can spread and even split the propagating mass in several small/medium sized deposits rather than in one single deposit, because of local topography and overall landslide dynamics during the propagation stage. Run-up of the landslide along the slopes on the opposite side of the valley also contributes to spread the moving mass towards different paths. Thus, it is not surprising that for source No. 3 the landslide with the smallest volume results in the highest dam. Even more, it is important to quantify case-by-case the specific scenario in relation to the most probable expected landslide volume, also including uncertainties in the propagation analysis.

A similar behavior as for source No. 2 can also be observed for source No. 4. While at the lowest landslide volume the deposit forms the steepest and most concentrated dam, with increasing volume the lateral spread of the material increases too, forming a shallower and wide landslide dam (Fig. 8). Then again, source No. 5 forms a relatively concentrated and steep landslide dam. It enters the main river channel through a small tributary gully, where at the lower volume most of the material remains in the tributary valley and blocks the stream channel there (Fig. 8). With increasing volume the landslide becomes more mobile and forms a high and steep dam in the main river channel, which is relatively narrow at that point. The same observations manifest in the boxplots used to compare the statistical distribution of the dam heights in each scenario (Fig. 9a). While the more mobile landslides form dams with a relatively narrow height distribution, the less mobile landslides form dams with a wider range in the size distribution. However, here the major part of the dam heights is below 20 m.

Figure 7.

Figure 8.

Figure 9.

Table 2.

Table 3.

5.2. Scenario evaluation

The relatively precise quasi-3D information about the spatial distribution of the simulated landslide dam heights allows a relatively thorough analysis of the shape of the resulting landslide dam and the completeness of blockage. The minimum and maximum dam height as well as the mean dam height were extracted along the points of blockage for the whole valley width W_V and the river channel width W_R (Fig. 9b and 9c, respectively). Here, in the cases where the minimum dam height exceeds the water level of the river (3-4 m), a complete blockage of the valley/river occurs. A complete river blockage occurs in all scenarios for sources No. 2 and 3, scenarios S4_a, S5_b, and S5_c, while a complete valley blockage occurs in scenarios S2_a, S2_c, S3_a, S3_a, and S4_b. However, a dam forming a stable impoundment can only be expected when the dam height exceeds the water table sufficiently. Interestingly, this is the case for all landslide scenarios with the lowest volume, S2_b, S3_b, S4_b, and S5_b. In addition, the shape of the landslide dam has a major effect on the longevity of the dam. While overtopping and subsequent breaching from erosion by the overtopping water is the most common dam failure mechanism (**Costa and Schuster 1988**), a higher, steeper dam is believed to be more susceptible to this kind of failure mechanism (**Ermini and Casagli 2003**). Another common failure mechanism is the internal erosion of the dam due to the high porosity of the often uncompacted material allowing for increased water seepage, a process referred to as piping (**Costa and Schuster 1988**). According to **Ermini and Casagli (2003)** piping is also controlled by the dam height, which influences the water table within the dam and the hydraulic gradient. Taking into account these insights, the scenarios forming wider and more massive dams, such as scenarios No. 2 and 4 can be considered as more stable dams and evaluated as more hazardous in terms of upstream flooding scenarios where full river blockages occur, while scenarios No. 3 and 5 form higher and steeper dams that are more susceptible to breaching and consequently more hazardous in terms of sudden dam breach and related outburst flood events. The reference case Baishuihe landslide actually formed a dam with a high size range and a quite high maximum dam height of 41.55 m. However, the majority of the dam is below 20 m, with a median dam height of only 5.2 m, so it can also be considered as a rather shallow and massive dam.

For the evaluation of landslide dam formation and evolution scenarios also different empirical geomorphological indices, the Blockage Index BI, Dimensionless Blockage Index DBI, the morphological obstruction index MOI, and the Hydromorphological Dam Stability Index HDSI, were employed. Domain thresholds as given above were used for the discrimination of dam formation and non-formation and dam stability scenarios, respectively. However, it should be considered that the separation performance of these relatively simple graphical methods used for the estimation of "critical" values is limited. The values are strictly empirical and they may vary and have to be modified for different regions (**Korup 2004**). Thus, here the computed values are also compared to the benchmark case of the Baishuihe landslide that formed a stable dam impounding the river until it was removed by the local authorities. The results of the computed inputs and indices are shown in Table 4, plotted on bi-logarithmic plots for BI and DBI in Fig. 10 and for MOI and HDSI in Fig. 11, and compared in a better perceivable way in Fig. 12.

Taking the BI as a first criterion for the scenario evaluation, for none of the simulated scenarios it reaches the formation domain with uncertain evolution. However, when comparing it to the BI of Baishuihe landslide all the cases with the highest landslide volume (c), and for sources No. 4 and No. 5 also the cases with the intermediate landslide volume (a) reach a higher BI than Baishuihe landslide and should thus have the potential to form a dam that can block the river.

According to the DBI and the classification of **Ermini and Casagli (2003)**, in none of the simulated scenarios a stable dam is formed. It basically decreases with increasing volume and decreasing dam height. The most unstable dams are formed by the two cases with the highest landslide dams, case No. 3_b and No. 4_b. In comparison, scenario S2_c, and all scenarios for source No. 4, form more stable dams than Baishuihe landslide according to the DBI. However, when looking at the simulated dam heights (Fig. 9), it occurs that apart from S4_b none of these cases produces a blockage exceeding the water level of the river. With this observation a weakness of the DBI for the prediction of future scenarios can be pointed out. With the index it is taken into account, that dams with large volumes and low dam heights tend to produce more stable dams, however, it is not considered that a minimum dam height is necessary to produce a blockage.

The MOI plots for all cases within the domain of landslide dam formation with uncertain evolution. For all scenarios it increases with increasing volume. With regard to the reference case representing a formed landslide dam with uncertain evolution, the MOI seems to be more suitable for the application to this case study than the BI and DBI, using the width of the valley as variable describing the properties of the blocked river as opposed to the catchment area. In the cases with the highest landslide volume, and for sources No. 4 and No. 5 in all cases, the MOI of Baishuihe landslide is exceeded, indicating that these cases have a higher potential than Baishuihe landslide to form a landslide dam. **Tacconi Stefanelli et al. (2016)** propose to use the HDSI to evaluate the stability of dams that were identified with the MOI as formed dams. For the HDSI, the simulated cases all plot within the instability domain. However, compared to the reference case, in all the cases where a dam formation was predicted by the MOI, the HDSI is also higher than that of the reference case, except for case No. 5_b. For scenario 5 the slope of the riverbed is actually higher than in all the other scenarios, leading to a lower HDSI and owing to the fact that the erosive power of the river is higher when the slope of the riverbed is steeper.

Table 4.

Figure 10.

Figure 11.

Figure 12.

In Table 5 the evaluation result for each criterion is summarized. Interestingly, the cases that lead to more complete blockages of the river and valley (S2 and S3), as evidenced by the spatial distribution of the simulated landslide deposits, are classified by the geomorphological indices as rather instable or even not formed landslide dams. Opposed to that, with the geomorphological indices the scenarios No. 4 and 5 are pointed out to produce the more stable dams, which might be due to the fact that for all indices the landslide volume is an input, which is higher in these scenarios. However, in most of these scenarios the river is not blocked by the landslide deposit. Taking into account both, the spatial distribution of the dam and the evaluation of the geomorphological indices, scenario S4_b seems to represent the most likely case of a stable and complete blockage of the river. Another case of a likely formation of a stable river blockage is S5_c. In this scenario a steep and high dam is formed, that might be subject to breaching when overtopped.

The behavior of flow-type landslides is strongly depending on the local topography, the volume of the propagating mass, and the overall landslide dynamics. Our simulation results show that even flow-type landslides propagating through the same gully can behave completely different during the deposition stage with strong variations in the mobility and shape of the final deposit. So even though the forward simulation with the GeoFlow_SPH code allows for a very precise prediction of the landslide propagation and deposition phenomena, the landslide behavior is also sensitive to differences in the boundary conditions, such as the local topography, which are hard to predict for future events. However, our case study shows a relatively comprehensive range of different possible scenarios, with mobile landslides forming more massive dams, landslides forming high and steep dams, complete and incomplete river blockages. These results also underline how the precise quasi-three-dimensional simulation of flow type landslide propagation with SPH numerical modeling enhances the interpretation of run-out models regarding river damming scenarios.

The power of geomorphological indices for landslide dam evolution assessment based on simple inputs such as estimates of landslide volumes is limited for landslides of the flow-type in two aspects. First, the values computed in this study are often far away from the domains given in the literature for the formation of landslide dams, while the spatial distribution of the simulated landslide deposits and the comparison with the reference case of a formed landslide dam indicate the formation of a river damming deposit. Thus, as other authors already pointed out before (e.g. **Korup 2004**), these formation domain thresholds should be adapted for different regions. Secondly, the spatial distribution of the landslide deposit cannot be accounted for, which is in the case of flow-type landslides highly variable and crucial for the blockage of a river. This seems to be particularly the case for the intermediate landslide volumes considered in our study that are close to the discrimination threshold of the dam formation domain.

Regardless of the stability of the formed landslide dams, it could be shown that in the wide range of simulated scenarios, the landslides are always deposited in the main river channel and thus have the potential for either forming a stable dam and causing an impoundment of the river and upstream flooding (e.g. scenarios S4_b and S5_c), or to form an incomplete or instable dam that might result in a sudden outburst flood downstream. Thus, it is advisable to carefully observe if further slumps form in the upper slope area, to enable a timely preparation of precautionary measures.

Table 5.

6. Conclusions

Landslide dams are a common phenomenon in mountainous areas where landslides are being deposited in river channels. Several hazardous phenomena can evolve from a landslide propagating into a river, such as the impoundment of the river and related upstream flooding in case a stable dam is formed, or the collapse of an unstable dam resulting in downstream flooding. The formation of a dam and its stability is depending on characteristics of the landslide deposit, such as the height, area, and volume, and characteristics of the river, such as valley and river channel width, river bed inclination, its discharge and erosive power.

We here proposed a methodology for assessing possible landslide dam evolution scenarios in a site-specific case study for landslides of the flow-type. In a first step landslide propagation is forward simulated for potential future landslide sources with SPH numerical modeling based on previously back-analyzed parameters of an occurred landslide on the same slope. In a second step the resulting landslide deposition volumes and shapes are evaluated regarding landslide dam formation and evolution in a qualitative assessment and with the help of empirical geomorphological indices employing characteristics of the landslide and the dammed river, such as the newly by **Tacconi Stefanelli et al. (2016)** developed Morphological Obstruction Index (MOI) and Hydrodynamic Dam

Stability Index (HDSI) index system.

Landslide propagation was simulated for four potential source zones with a variation of three different triggering volumes, respectively. It turned out that in all scenarios the major part of the landslide is deposited in the river valley. The mobility of the landslide was usually increasing with increasing triggering volume. The landslide dynamics and the shape of the resulting deposit are strongly depending on the particular local topography and landslide parameters. In two scenarios the landslides were more mobile and formed rather shallow, wide, and massive deposits, while in the two other scenarios high and steep landslide deposits were formed.

In the assessment of the deposition shapes and their spatial distribution several cases could be identified where a complete blockage of the river channel or even the entire valley width occurred. In these cases the formation of a landslide dam can be assumed that can either form a stable impoundment or breach at some point. It is generally assumed that a more shallow and massive dam can reach a higher long-term stability than a steep and high dam, given that the height of the river level is sufficiently exceeded. The here for the first time for the prediction of landslide propagation and river blocking scenarios employed SPH numerical modeling approach proved to be powerful for the assessment of scenarios by providing precise quasi-three-dimensional information about the geometry of the modeled landslide deposits.

Then the landslide dams were classified with the help of empirical geomorphological indices and thresholds for domains of landslide dam formation and non-formation based on values proposed in the literature. With the computed indices none of the simulated cases, but also not the reference back-analysis case, could be identified as formed stable dams. This underlines the necessity of adapting the empirical thresholds for particular settings. The indices for the benchmark case with a formed stable dam were subsequently used as a reference to compare to the simulated cases. The Dimensionless Blockage Index (DBI), which employs the dam volume and height as well as the area of the catchment upstream of the point of blockage as a measure for the erosive power of the river, identifies most of the rather massive landslide deposits as stable. The Blockage Index (BI) and the Morphological Obstruction Index (MOI) on the other hand, employing only the volume as characteristic describing the landslide dam tend to identify landslides with a higher volume as more stable. In several cases the results of the indices are in contradiction to the identification of complete river blockings, underlining the limitations of the empirical methods for site-specific cases, supposedly particularly for cases of intermediate landslide volumes that are near the discrimination thresholds.

Acknowledgements

The authors would like to thank the support of the National Natural Science Foundation of China (Grant No. 41402285 and Grant No. 41650110487) and the Chinese Academy of Sciences President's International Fellowship Initiative (Grant No. 2016PZ032). Prof. Manuel Pastor (Universidad Politecnica de Madrid, Spain) and co-workers are much acknowledged for having provided the "GeoFlow_SPH" code used for the numerical simulations.

References

Blanc T (2008) Numerical simulation of debris flows with the 2D SPH depth-integrated model. Master's thesis, Institute for Mountain Risk Engineering, University of Natural Resources and Applied Life Sciences, Vienna, Austria.

Blanc T, Pastor M, Drempetic MSV, Haddad B (2011) Depth integrated modelling of fast landslides propagation. European Journal of Environmental and Civil Engineering 15:51-72.

Braun A, Wang X, Petrosino S, Cuomo S (2017) SPH propagation back-analysis of Baishuihe landslide in south-western China. Geoenvironmental Disasters, 4(1), 2.

Canuti P, Casagli N, Ermini L (1998) Inventory of landslide dams in the Northern Apennine as a model for induced flood hazard forecasting. In: Andah K (Ed.), Managing Hydrogeological Disasters in a Vulnerable Environment for Sustainable Development CNR-GNDCI Publication Vol. 1900. CNR-GNDCI-UNESCO (IHP), Perugia, pp. 189-202.

Cascini L, Cuomo S, Pastor M, Sorbino G, Piciullo L (2014) SPH run-out modelling of channelised landslides of the flow type. Geomorphology 214: 502-513.

Cascini L, Cuomo S, Pastor M, Rendina I (2016) SPH-FDM propagation and pore water pressure modelling for debris flows in flume tests. Engineering Geology 213: 74-83.

Corominas J, Van Westen C, Frattini P, Cascini L, Malet JP, Fotopoulou S, Catani F, Van Den

Eeckhaut M, Mavrouli O, Agliardi F, Pitilakis K, Winter MG, Pastor M, Ferlisi S, Tofani V, Hervás J, Smith JT (2014) Recommendations for the quantitative analysis of landslide risk. Bulletin of Engineering Geology and the Environment 73(2): 209-263.

Costa JE, Schuster RL (1988) The formation and failure of natural dams. Geological Society of America Bulletin 100(7): 1054-1068.

Cuomo S (2014) New Advances and Challenges for Numerical Modeling of Landslides of the Flow Type. Procedia of Earth and Planetary Science. 9: 91-100.

Cuomo S, Pastor M, Capobianco V, Cascini L (2016) Modelling the space–time evolution of bed entrainment for flow-like landslides. Engineering Geology 212: 10-20.

Cuomo S, Pastor M, Cascini L, Castorino GC (2014) Interplay of rheology and entrainment in debris avalanches: a numerical study. Canadian Geotechnical Journal, 51(11): 1318-1330.

Cuomo S, Pastor M, Vitale S, Cascini L (2013) Improvement of irregular DTM for SPH modelling of flow-like landslides. Proc. of XII International Conference on Computational Plasticity. Fundamentals and Applications (COMPLAS XII), Oñate E, Owen DRJ, Peric D, Suárez B (Eds). 3-5 September 2013, Barcelona, Spain. ISBN: 978-84-941531-5-0, pp. 512-521.

Deng B, Liu SG, Enkelmann E, Li ZW, Ehlers TA, Jansa L (2014) Late Miocene accelerated exhumation of the Daliang Mountains, southeastern margin of the Tibetan Plateau. International Journal of Earth Sciences. 104(4), 1-21.

Ermini L, Casagli N (2003) Prediction of the behavior of landslide dams using a geomorphical dimensionless index. Earth Surface Processes and Landforms 28, 31-47.

Fan X, Rossiter DG, Westen CJ, Xu Q, Görüm T (2014) Empirical prediction of coseismic landslide dam formation. Earth Surface Processes and Landforms, 39(14), 1913-1926.

Fan X, van Westen CJ, Xu Q, Gorum T, Dai F (2012) Analysis of landslide dams induced by the 2008 Wenchuan earthquake. Journal of Asian Earth Sciences. 57, 25-37.

Fan X, Xu Q, van Westen CJ, Huang R, Tang R (2017) Characteristics and classification of landslide dams associated with the 2008 Wenchuan earthquake. Geoenvironmental Disasters, 4(1), 12.

Fell R, Corominas J, Bonnard C, Cascini L, Leroi E, Savage WZ (2008) Guidelines for landslide susceptibility, hazard and risk zoning for land-use planning. Engineering Geology, 102(3), 99-

111.

Gingold RA, Monaghan JJ (1977). Smoothed particle hydrodynamics: theory and application to non-spherical stars. Monthly Notices of the Royal Astronomical Society 181(3): 375-389.

Huang Y, Zhang W, Xu Q, Xie P, Hao L (2012). Run-out analysis of flow-like landslides triggered by the Ms 8.0 2008 Wenchuan earthquake using smoothed particle hydrodynamics. Landslides, 9(2), 275-283.

Hungr O, Leroueil S, Picarelli L (2014) The Varnes classification of landslide types, an update. Landslides, 11(2), 167-194.

Hutchinson JN (1986) A sliding-consolidation model for flow slides. Canadian Geotechnical Journal 23(2): 115–126.

JAXA (2016) ALOS Global Digital Surface Model 'ALOS World 3D – 30m' (AW3D30 DSM Ver. 1.0), data available from the Japanese Aerospace Exploration Agency (JAXA) web interface, http://www.eorc.jaxa.jp/ALOS/en/aw3d30/data/index.htm, accessed on 14 November, 2016.

Korup O (2004) Geomorphometric characteristics of New Zealand landslide dams. Eng. Geol. 73 (1), 13-35.

Lucy LB (1977) A numerical approach to the testing of the fission hypothesis. The Astronomical Journal 82: 1013-1024.

McDougall S, Hungr O (2004) A model for the analysis of rapid landslide motion across three-dimensional terrain. Canadian Geotechnical Journal 41(6): 1084-1097.

Okeke ACU, Wang F (2016) Critical hydraulic gradients for seepage-induced failure of landslide dams. Geoenvironmental Disasters, 3(1), 9.

Pastor M, Crosta GB (2012) Landslide runout: Review of analytical/empirical models for subaerial slides, submarine slides and snow avalanche. Numerical modelling. Software tools, material models, validation and benchmarking for selected case studies. Deliverable D1.7 for SafeLand Project http://www.safeland-fp7.eu/results/Documents/D1.7_revised.pdf., 2012.

Pastor M, Quecedo M, Fernández-Moredo JA, Herreros MI, González E, Mira P (2002) Modelling tailings dams and mine waste dumps failures. Géotechnique 52: 579-591.

Pastor M, Haddad B, Sorbino G, Cuomo S, Drempetic V (2009) A depth-integrated, coupled SPH model for flow-like landslides and related phenomena. International Journal for Numerical and Analytical Methods in Geomechanics, 33, 143-184.

Pastor M, Blanc T, Haddad B, Petrone S, Morles MS, Drempetic V, Issler D, Crosta GB, Cascini L, Sorbino G, Cuomo S (2014) Application of a SPH depth-integrated model to landslide run-out analysis. Landslides 11(5): 793-812.

Peng M, Zhang LM (2012) Breaching parameters of landslide dams. Landslides 9 (1), 13-31.

Pirulli M, Pastor M (2012) Numerical study on the entrainment of bed material into rapid landslides. Géotechnique 62(11): 959-972.

Swanson FJ, Oyagi N, Tominaga M (1986) Landslide dams in Japan. In: Schuster RL (Ed.), Landslide Dams: Processes Risk and Mitigation. Geotechnical Special Publication Vol. 3. American Society of Civil Engineering, New York, pp. 131-145.

Tacconi Stefanelli C, Catani F, Casagli N (2015) Geomorphological investigations on landslide dams. Geoenvironmental Disasters 2 (1), 1-15.

Tacconi Stefanelli C, Segoni S, Casagli N, Catani F (2016) Geomorphic indexing of landslide dams evolution. Engineering Geology 208, 1-10.

USGS (2015) SRTM 1 Arc-Second Global elevation data, data available from the U.S. Geological Survey (USGS) via the EarthExplorer web interface, https://earthexplorer.usgs.gov/, accessed on 7 February, 2017.

Table 1. Rheological parameters of Baishuihe landslide estimated in the back-analysis using the "GeoFlow_SPH" code (**Braun et al. 2017**)

H_{trig} (m)	V_{in} (m^3)	h_w^{rel} (-)	p_w^{rel} (-)	c_v (m^2s^{-1})	K (-)	V_{fin} (m^3)	L (m)	H_{med} (m)
15	550125	0.5	0.6	1.0×10^{-2}	0.006	912255	615	11

H_{trig}: height of triggering mass; V_{in}: initial volume, h_w^{rel}: relative water height, p_w^{rel}: ratio of pore water pressure to liquefaction pressure; c_v: consolidation factor, K: empirical parameter for the bed entrainment law of Blanc et al. (2011); V_{fin}: final volume; L: width of deposition zone; H_{med}: mean deposition height.

Table 2. Modeled run-out distances and dam dimensions

Case No.	V_i	V_f	V_d	Max H_d	Mean H_d	Median H_d	W_d
	m^3	m^3	m^3	m	m	m	m
BSH	550125	912255	912255	41.5	10.7	5.2	615
S2_b	362750	559749	559749	30.8	10.6	10.0	340
S2_a	544125	835558	835558	18.2	5.9	5.6	800
S2_c	725500	1096641	1096641	14.2	4.8	4.5	1040
S3_b	362000	640565	640565	40.3	13.5	13.4	370
S3_a	543000	873640	873640	44.8	11.6	6.2	580
S3_c	724000	1106859	1106859	50.9	12.8	7.1	650
S4_b	365500	805340	791122	27.3	5.7	4.1	900
S4_a	548250	1228343	1205474	23.3	5.0	3.2	1300
S4_c	731000	1656296	1576296	13.9	3.7	3.1	1610
S5_b	361000	1520191	616771	44.5	10.4	8.2	580
S5_a	541500	1879605	1070055	53.5	12.0	8.0	650
S5_c	722000	2416227	2178147	42.6	16.9	16.8	650

h_{trig}: triggering height, V_i: initial volume landslide, V_f: final volume landslide, V_d, volume dam, H_d: height dam, Max H_d: maximum height dam, Mean H_d: mean height dam, Median H_d: median height dam W_d: width dam

Table 3. Simulated minimum, maximum, and mean dam heights along the blocked valley and river channel cross section, respectively

Case No.	Along valley width W_V			Along river channel width W_R		
	Min H_d m	Max H_d m	Mean H_d m	Min H_d m	Max H_d m	Mean H_d m
BSH	0.0	41.2	16.3	18.9	41.2	32.3
S2_b	2.9	24.7	12.1	9.0	23.6	14.1
S2_a	5.1	16.3	7.8	5.1	15.5	8.3
S2_c	5.5	13.4	8.6	5.5	10.8	7.0
S3_b	12.1	38.3	21.1	13.8	37.3	20.2
S3_a	7.7	44.5	22.2	8.4	43.7	21.7
S3_c	0.0	49.5	19.0	5.8	48.9	22.4
S4_b	4.8	16.5	12.7	14.0	16.4	15.3
S4_a	3.0	5.1	4.6	3.1	5.0	4.4
S4_c	0.0	5.5	2.5	0.0	5.6	4.2
S5_b	0.0	20.2	7.6	13.5	20.2	17.1
S5_a	0.0	46.2	11.6	0.0	45.9	14.2
S5_c	0.0	40.3	9.9	16.5	36.2	26.1

Min H_d: minimum height dam, Max H_d: maximum height dam, Mean H_d: mean height dam

Table 4. Geomorphological characteristics of the river and computed landslide dam stability indices

Case No.	W_v m	W_R m	S m/m	A_b km^2	MOI	HDSI	BI	DBI
BSH	139	64	0.0143	2244.5	3.82	4.45	2.61	4.11
S2_b	169	110	0.0175	2248.2	3.52	4.15	2.40	4.60
S2_a	169	110	0.0175	2248.2	3.69	4.33	2.57	4.18
S2_c	169	110	0.0175	2248.2	3.81	4.45	2.69	3.96
S3_b	169	110	0.0175	2248.2	3.58	4.21	2.45	4.67
S3_a	169	110	0.0175	2248.2	3.71	4.35	2.59	4.20
S3_c	169	110	0.0175	2248.2	3.82	4.45	2.69	4.16
S4_b	119	59	0.0079	2249.9	3.83	4.66	2.55	4.07
S4_a	146	70	0.0079	2245.9	3.92	4.84	2.73	3.78
S4_c	189	102	0.0079	2250.2	3.94	4.97	2.85	3.65
S5_b	165	40	0.0262	2271.2	3.96	4.41	2.43	4.48
S5_a	165	40	0.0262	2271.2	4.06	4.50	2.67	4.23
S5_c	165	40	0.0262	2271.2	4.17	4.61	2.98	4.24

W_V: valley width, W_R: river width, S: local slope of river bed, A_b: catchment area, BI: Blockage Index, DBI: Dimensionless Blockage Index, MOI: Morphological Obstruction Index, HDSI: Hydromorphological Dam Stability Index.

Table 5. Multi-criteria comparison of all scenarios, with red color indicating a full blockage/stable dam, respectively, and green color indicating an incomplete blockage/unstable dam, respectively

	blockage river	blockage valley	shape	BI	DBI	MOI	HDSI
BSH	y	n					
S2_b	y	y	massive	n	n	n	n
S2_a	y	y	massive	n	n	n	n
S2_c	y	y	massive	y	y	n	n
S3_b	y	y	steep	n	n	n	n
S3_a	y	y	steep	n	n	n	n
S3_c	y	n	steep	y	n	y	y
S4_b	y	y	massive	n	y	y	y
S4_a	n	n	massive	y	y	y	y
S4_c	n	n	massive	y	y	y	y
S5_b	y	n	steep	n	n	y	n
S5_a	n	n	steep	y	n	y	y
S5_c	y	n	steep	y	n	y	y

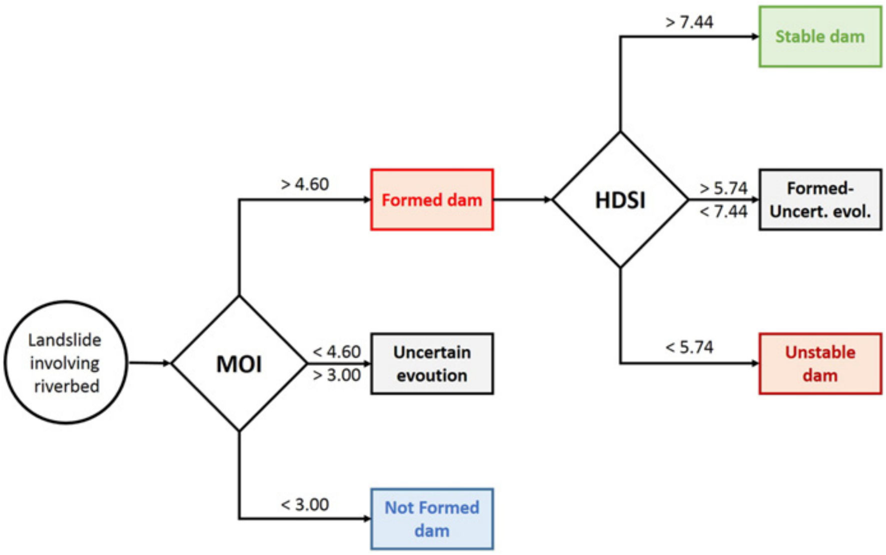

Fig. 1. Flow-chart for scenario evaluation from Tacconi Stefanelli et al. (2016)

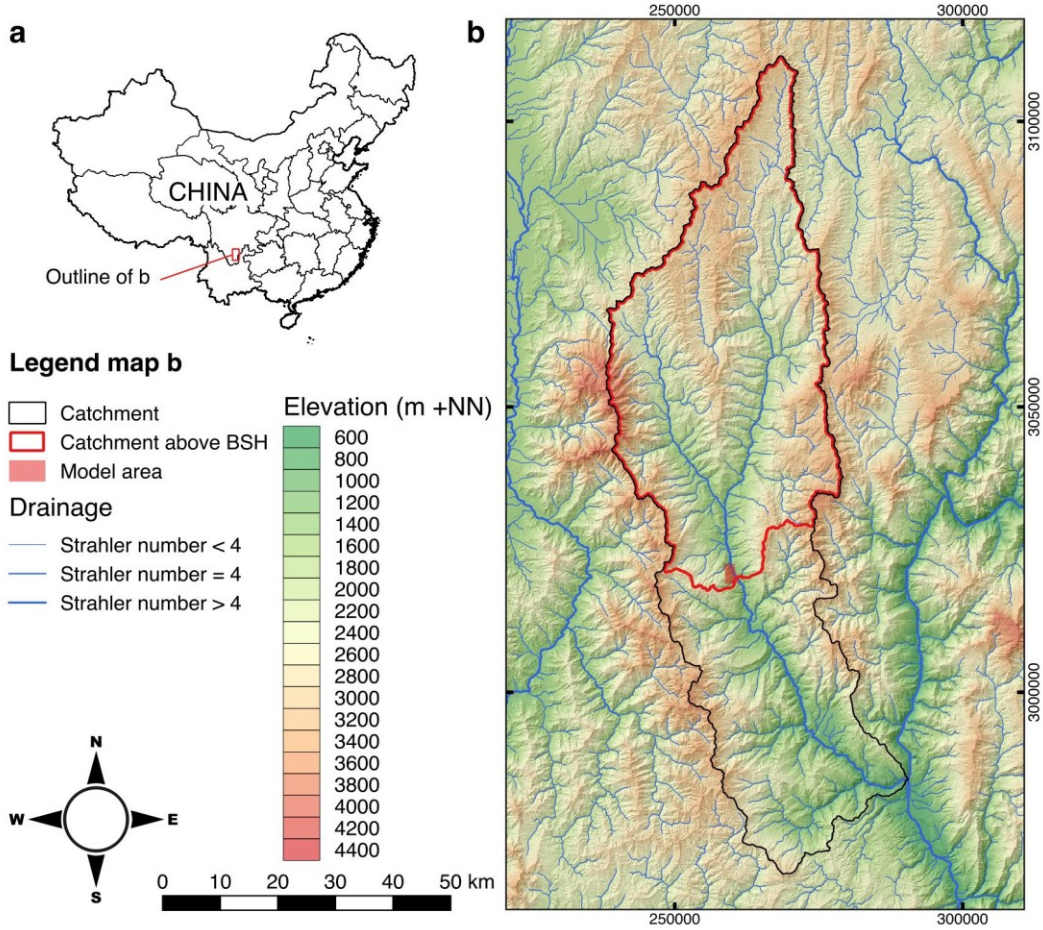

Fig. 2. Location of the study area in China (a), catchment, drainage system and location of the model area (b). Elevation data with 30 m resolution, ALOS World 3D – 30m (AW3D30) from JAXA (2016), voids filled with 30 m SRTM-1 data from USGS (2015)

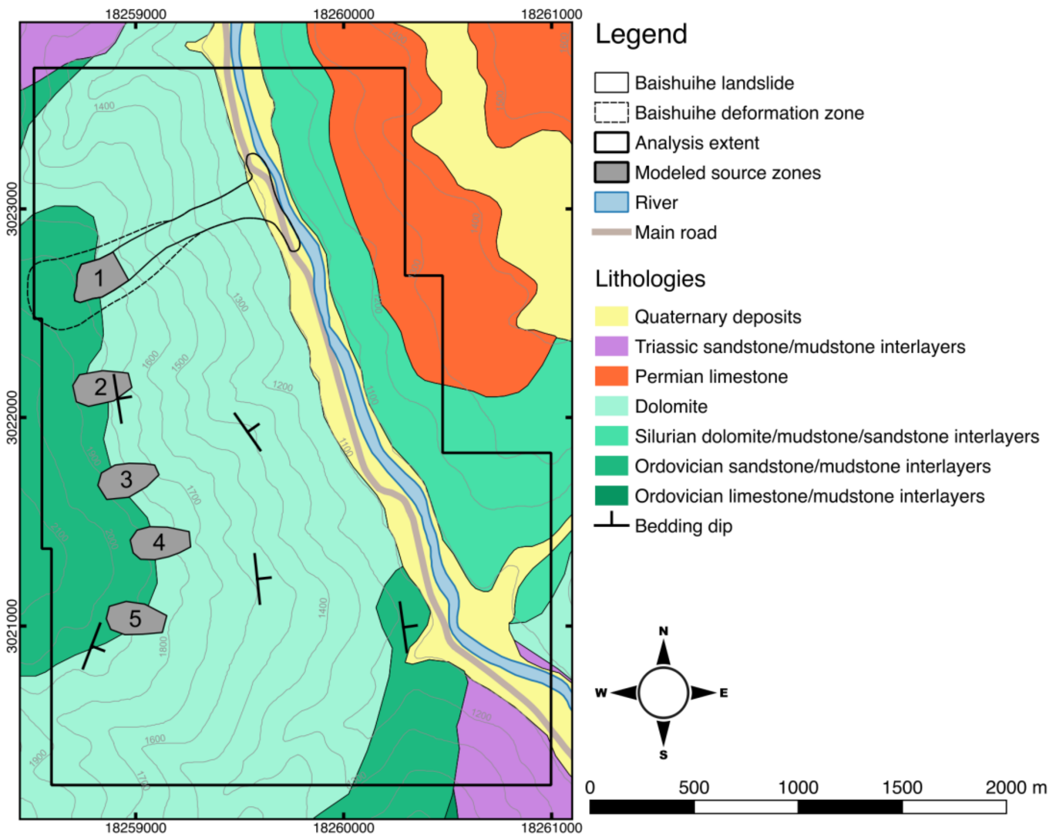

Fig. 3. Lithological map of the modeled slope, modeled source zone, outlines and deformation zone of Baishuihe landslide, and assumed source zones for forward-analyses

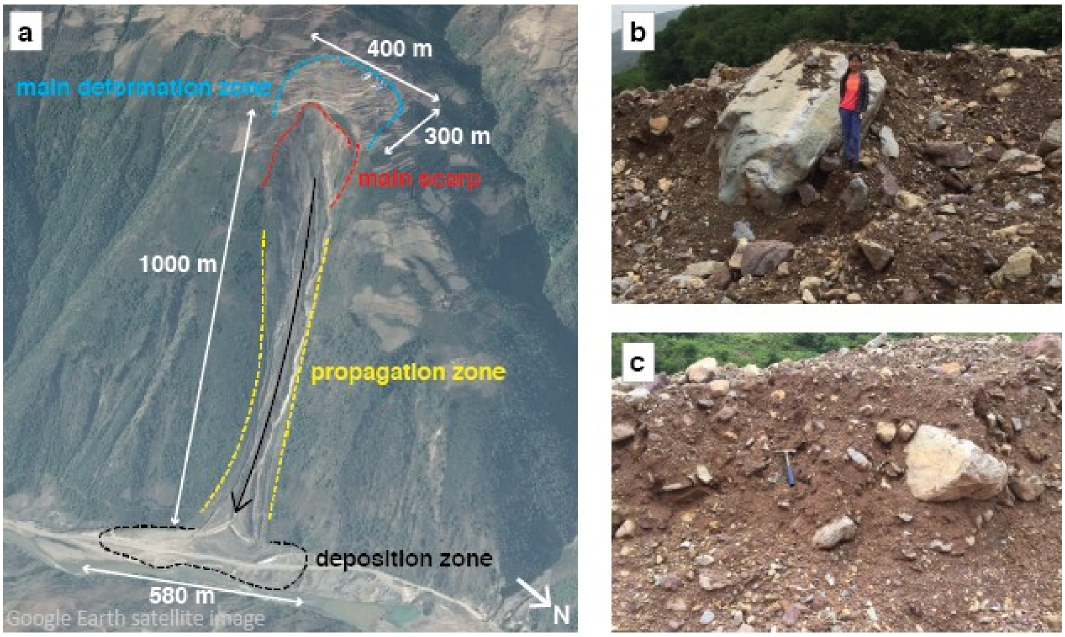

Fig. 4. Satellite image with main characteristics of Baishuihe landslide (a) and internal structure of the landslide deposit (b, c)

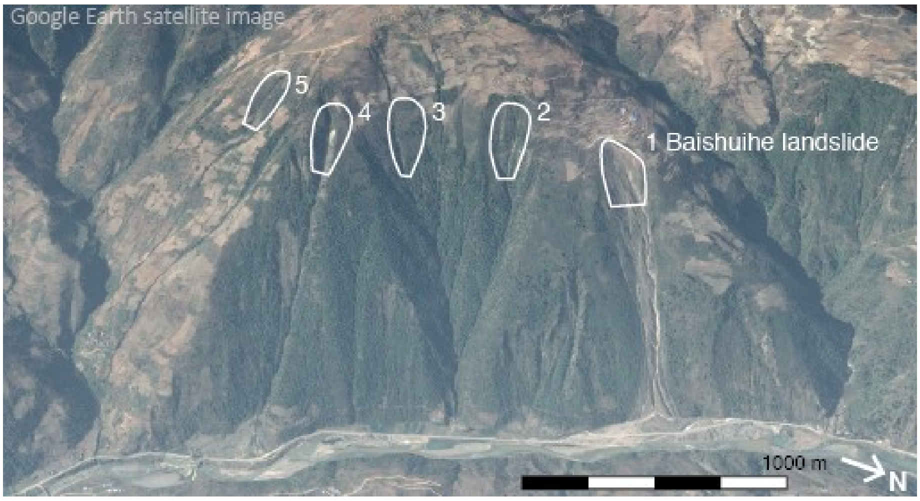

Fig. 5. Satellite image of the modeled source zones

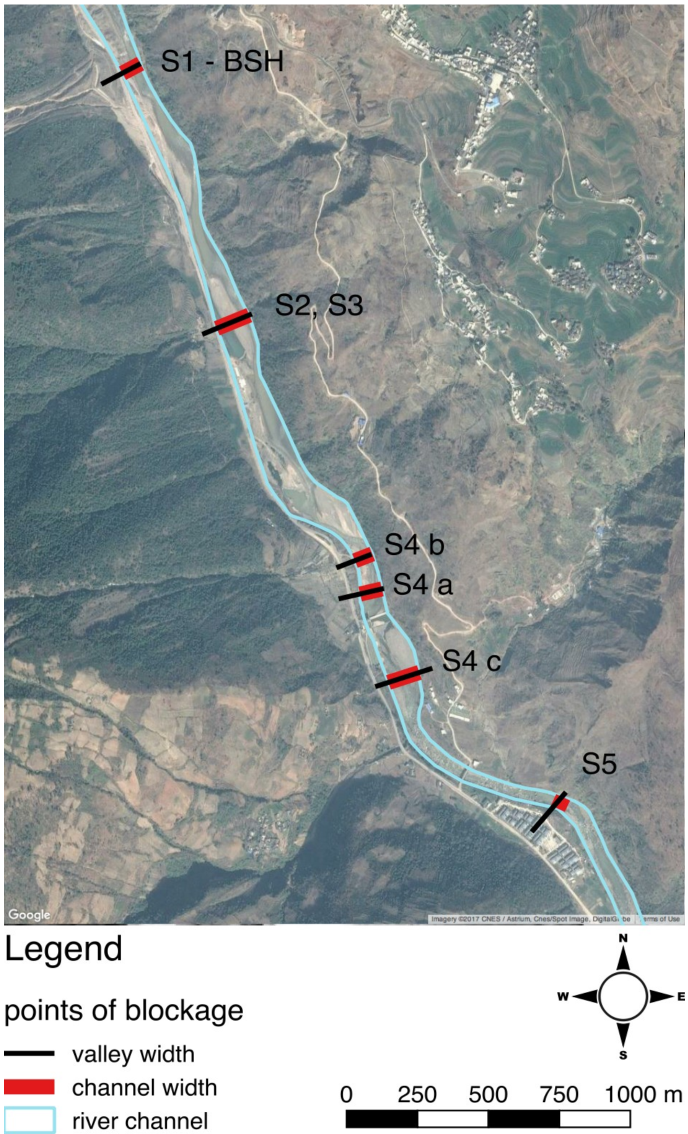

Fig. 6. Locations of the points of blockage in the different scenarios and the corresponding measurements of the river channel width (red line) and valley with (black line)

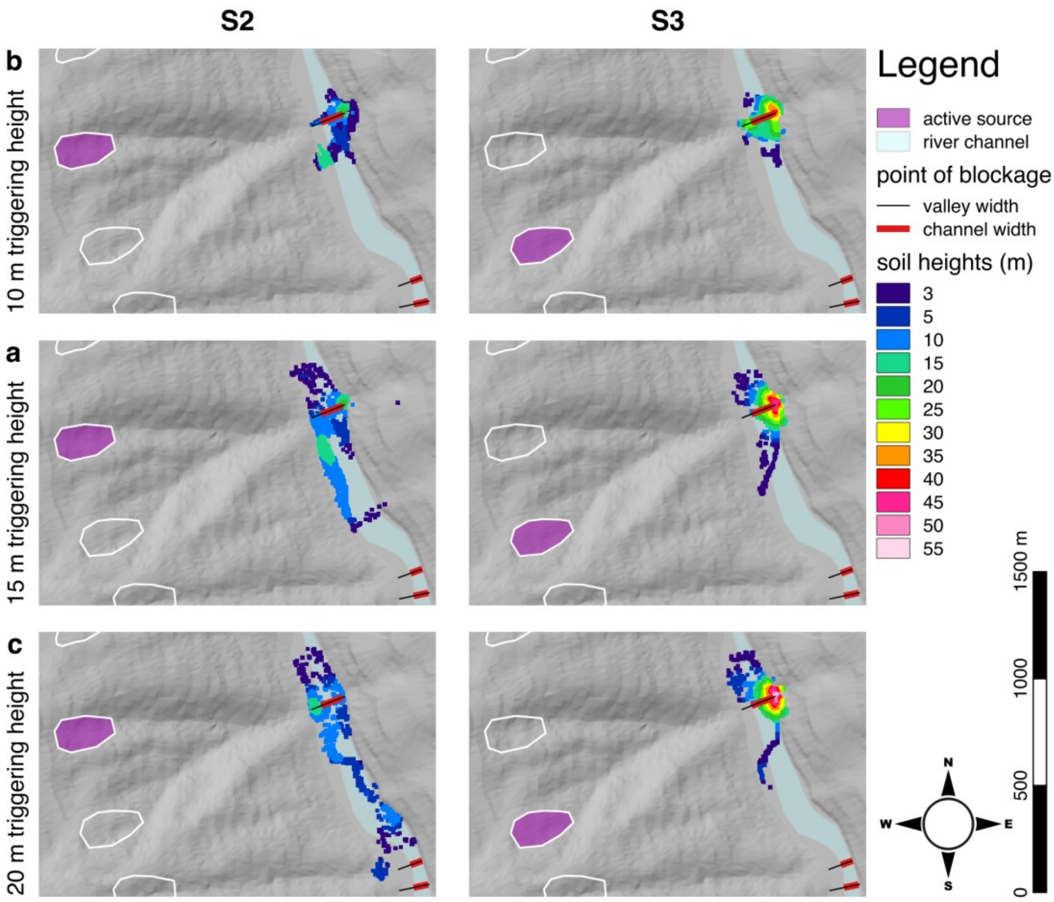

Fig. 7. Simulated heights of soil deposits with the indication of the landslide source zones for the simulated cases S2 and S3 and the river channel bed (bank-full river)

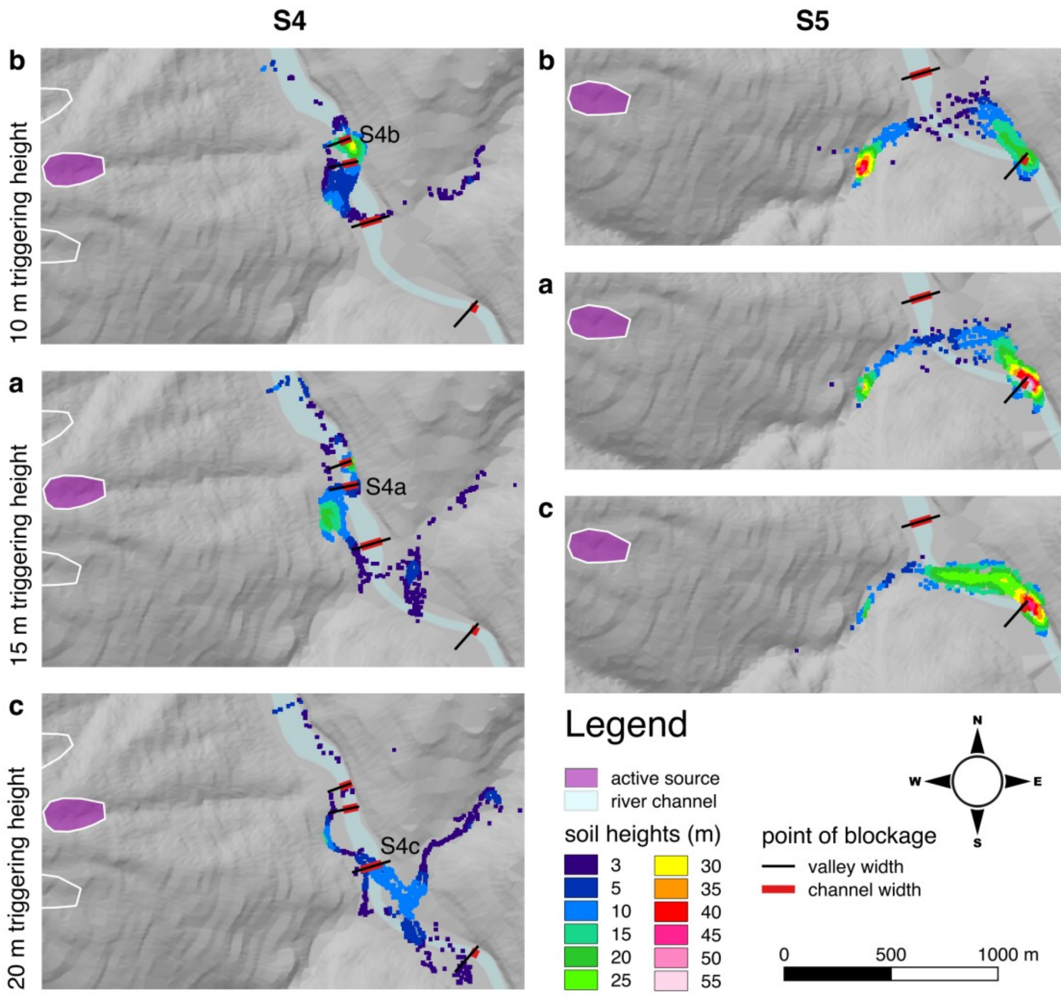

Fig. 8. Simulated heights of soil deposits with the indication of the landslide source zones for the simulated cases S4 and S5 and the river channel bed (bank-full river)

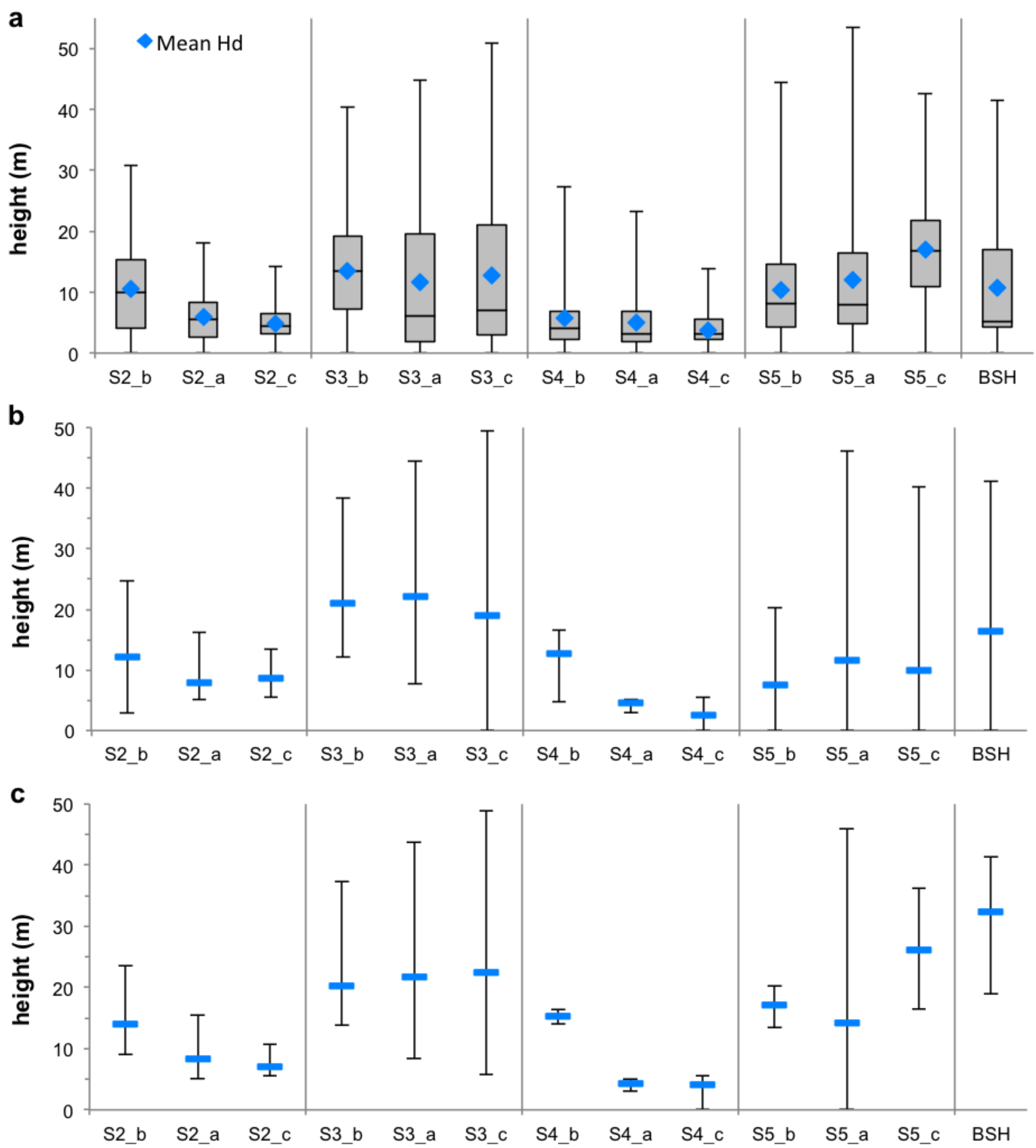

Fig. 9. Boxplots of the simulated resulting dam heights (a), where the upper whisker represents the maximum dam height, the lower whisker the minimum dam height, the upper boundary of the box the third quartile, the lower boundary the first quartile, the middle line representing the median, and the blue hash the mean dam height. Dam heights measured along the points of blockage (Fig. 6) with minimum and maximum dam height (upper and lower whisker), and mean dam height (blue marker) along the whole valley width (b) and the river channel width (c), respectively

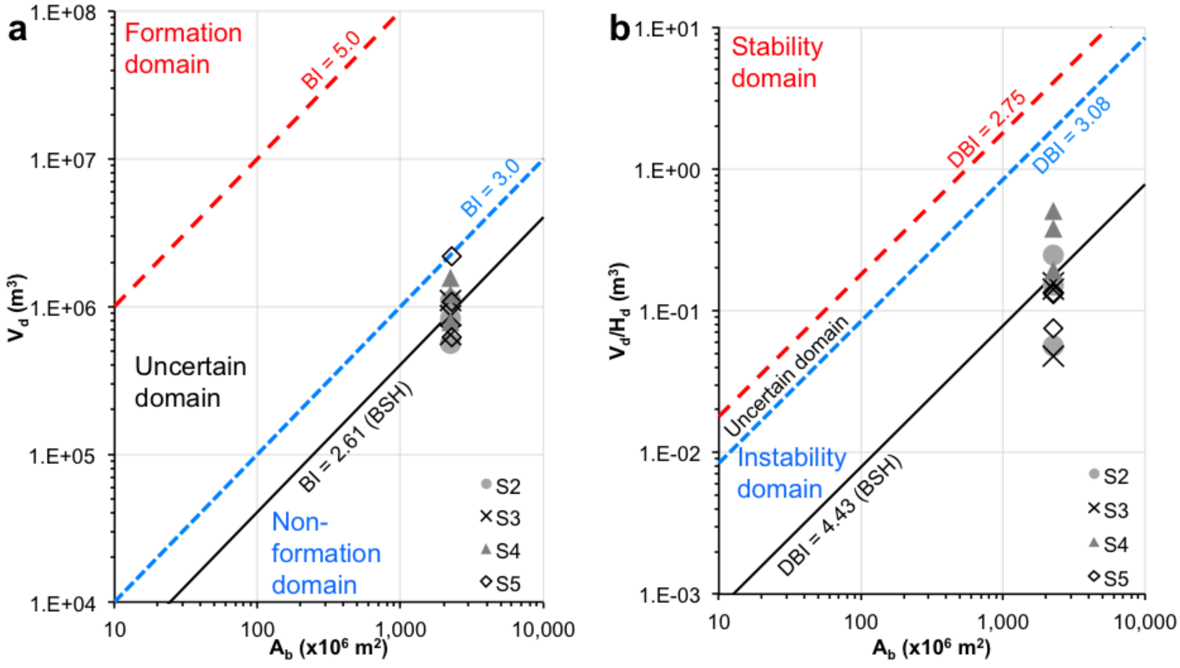

Fig. 10. Bi-logarithmic plots for Blockage Index (BI) and Dimensionless Blockage Index (DBI) with domain differentiation after **Ermini and Casagli (2003)**

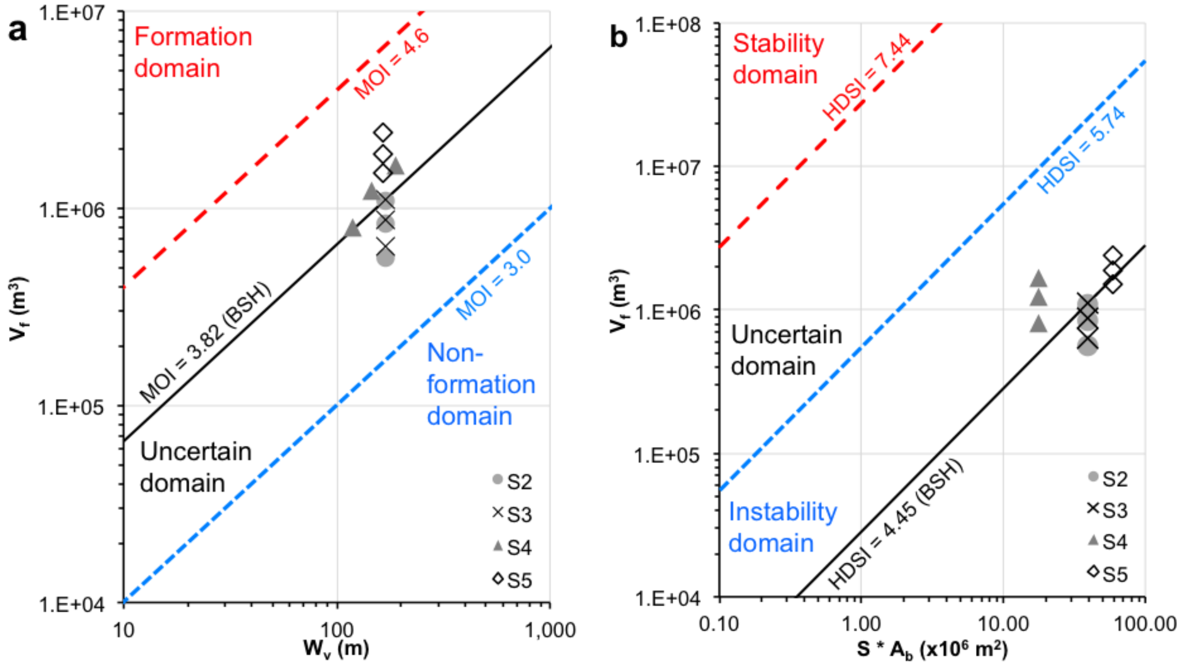

Fig. 11. Bi-logarithmic plots for Morphological Obstruction Index (MOI) and Hydromorphological Dam Stability Index (HDSI) with domain thresholds as proposed by **Tacconi Stefanelli et al. (2016)**

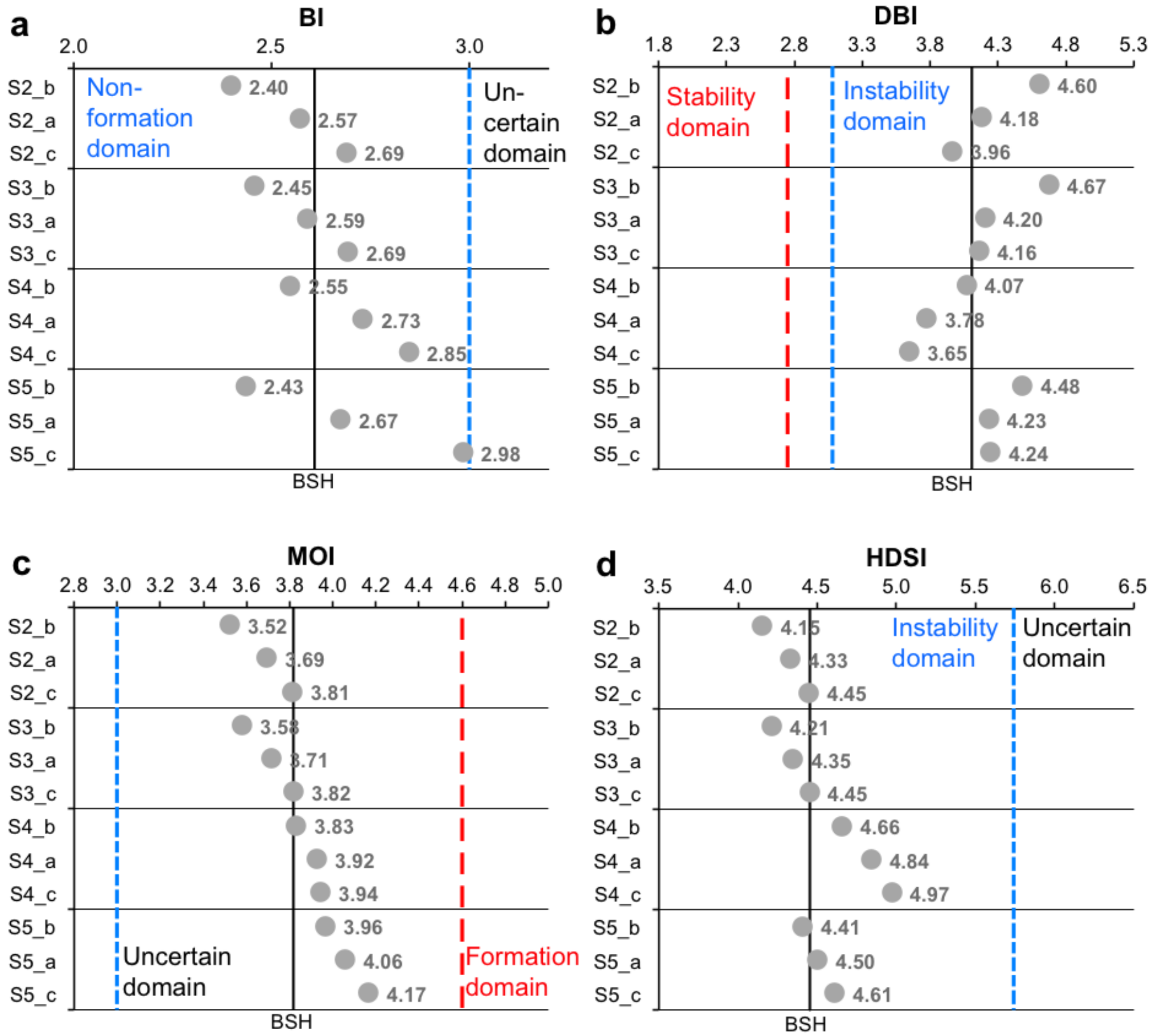

Fig. 12. Plots of the calculated geomorphological dam evolution indices blockage index BI (a), dimensionless blockage index DBI (b), morphological obstruction index MOI (c) and hydromorphological dam stability index HDSI (d)